ACS APPLIED ENERGY MATERIALS

www.acsaem.org Letter

Enhanced Charge Carrier Separation in $WO_3/BiVO_4$ Photoanodes Achieved via Light Absorption in the $BiVO_4$ Layer

Ivan Grigioni,* Annalisa Polo, Maria Vittoria Dozzi, Kevin G. Stamplecoskie, Danilo H. Jara, Prashant V. Kamat, and Elena Selli*

Cite This: *ACS Appl. Energy Mater.* 2022, 5, 13142−13148 Read Online

ACCESS | Metrics & More | Article Recommendations | Supporting Information

ABSTRACT: Photoelectrochemical (PEC) water splitting converts solar light and water into oxygen and energy-rich hydrogen. $WO_3/BiVO_4$ heterojunction photoanodes perform much better than the separate oxide components, though internal charge recombination undermines their PEC performance when both oxides absorb light. Here we exploit the $BiVO_4$ layer to sensitize WO_3 to visible light and shield it from direct photoexcitation to overcome this efficiency loss. PEC experiments and ultrafast transient absorption spectroscopy performed by frontside (through $BiVO_4$) or backside (through WO_3) irradiating photoanodes with different $BiVO_4$ layer thickness demonstrate that irradiation through $BiVO_4$ is beneficial for charge separation. Optimized electrodes irradiated through $BiVO_4$ show 40% higher photocurrent density compared to backside irradiation.

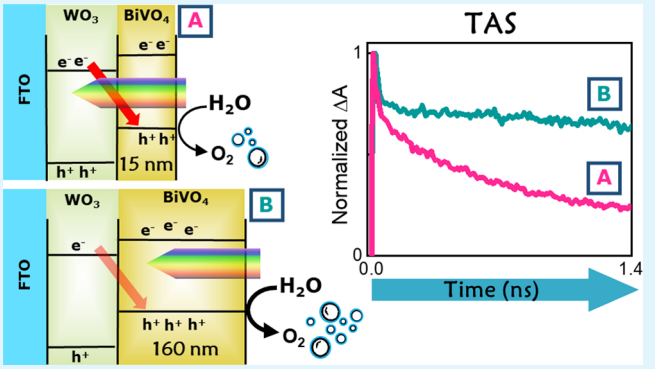

KEYWORDS: *solar water oxidation, heterojunction, ultrafast transient absorption, photoactive layer thickness, filter effect*

Bismuth vanadate, $BiVO_4$, is a promising semiconductor oxide employed in photoanodes for the oxygen evolution reaction in water-splitting devices.[1,2] Its stability in contact with aqueous electrolytes,[3,4] its good visible light-harvesting capability,[5] and its simple preparation through cheap wet techniques[6] point to this material as a possible component of future commercial photoelectrochemical (PEC) cells. Furthermore, in the last 15 years the efficiency of $BiVO_4$-based photoanodes (in terms of current density) rapidly grew from a few microamps per square centimeter in early reports to 4−5 mA cm^{-2}, with prolonged continuous operation of photoelectrodes modified with oxygen evolution cocatalysts.[3,4,6−13] However, the fast charge recombination of $BiVO_4$-based electrodes still hampers the efficiency of this material.[2,14]

A way to overcome this intrinsic flaw is to couple $BiVO_4$ with WO_3 in the $WO_3/BiVO_4$ heterojunction where visible light harvesting $BiVO_4$ sensitizes wider band gap WO_3.[15] $BiVO_4$ photoanodes based on this heterojunction achieve the highest current densities among oxide-based photoanodes.[16,17] The suitable band gap alignment between the two oxides, the efficient electron and hole transport in WO_3 and $BiVO_4$, respectively, and the spacial charge separation support the high performance of $WO_3/BiVO_4$ photoanodes.[18−25]

In previous studies, we investigated the charge carrier dynamics in the $WO_3/BiVO_4$ system through transient absorption spectroscopy (TAS) with detection either in the visible range to observe the hole dynamics in $BiVO_4$[18,26−28] or in the mid-infrared to follow the electron dynamics in WO_3 and $BiVO_4$.[29] We also identified wavelength-dependent processes by tuning the excitation wavelength across the WO_3 absorption edge (ca. 450 nm).[18,26,29] Indeed, the type II band alignment between the two oxides (Figure 1A) allows distinct charge transfer processes leading to charge separation or recombination, depending on the excitation wavelength. Under visible light excitation of $BiVO_4$, electrons promoted in its conduction band (CB) flow into the energetically lower-lying CB of WO_3, while holes remain in the $BiVO_4$ valence band (VB). This electron transfer process (process Ⓐ in Figure 1A) decreases charge recombination and leads to long-living charge carriers that are beneficial for PEC performance.[29]

Conversely, irradiation at wavelengths below 450 nm leads to the excitation of both oxides and opens a detrimental recombination path between the electrons photopromoted in the CB of WO_3 and the holes in $BiVO_4$ (process Ⓑ in Figure 1A). This process results in charge recombination on a ∼200 ps time scale[26] and becomes more relevant with increasing WO_3 layer thickness.[30]

Received: August 12, 2022
Accepted: October 11, 2022
Published: October 17, 2022

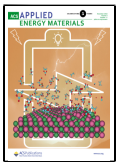

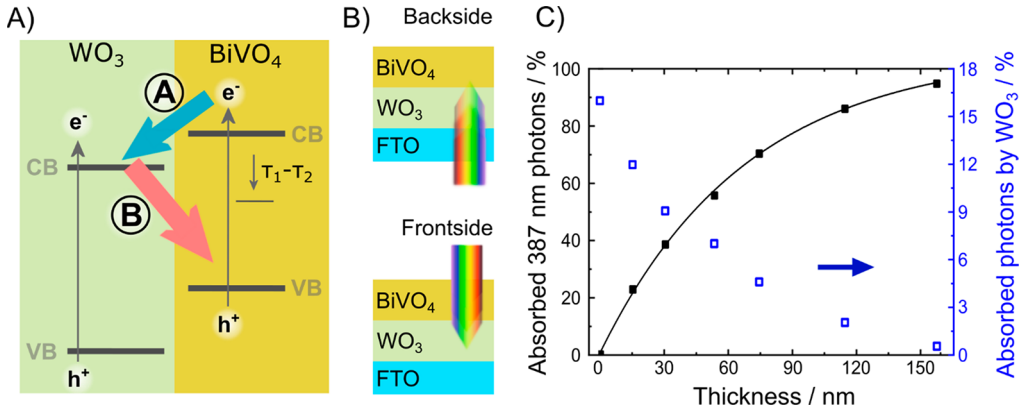

Figure 1. (A) Charge carrier transfer paths involved in the $WO_3/BiVO_4$ heterojunction: light absorption in $BiVO_4$ produces valence band (VB) holes h^+ and conduction band (CB) electrons e^-, which can recombine with holes (with time constants τ_1 and τ_2) or flow into WO_3 through process Ⓐ, leading to charge separation. When WO_3 is also photoexcited, electrons in its CB can recombine with holes in $BiVO_4$ through process Ⓑ. (B) Backside (through WO_3) and frontside (through $BiVO_4$) irradiation modes of the $WO_3/BiVO_4$ heterojunction photoanodes. (C) Percent amount of 387 nm photons (the pump wavelength used in TAS experiments) absorbed by the $BiVO_4$ layer (left ordinate) and by the WO_3 layer (right ordinate) under frontside excitation vs the thickness of the $BiVO_4$ layer in $WO_3/BiVO_4$ photoanodes.

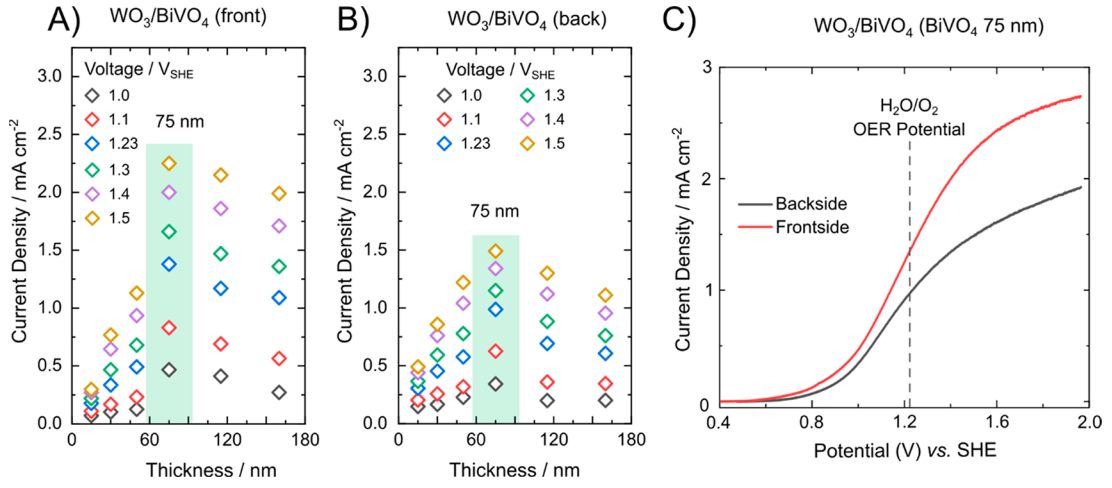

Figure 2. Current density generated under 1 sun simulated solar light (AM 1.5 G irradiation) at different applied potentials with the $WO_3/BiVO_4$ heterojunction electrodes in contact with a 0.5 M Na_2SO_4 aqueous solution under (A) frontside and (B) backside irradiation; (C) linear sweep voltammetry recorded with the best performing $WO_3/BiVO_4$ electrode (with a 75 nm thick $BiVO_4$ layer) under backside (black line) and frontside (red line) irradiation; the vertical dashed line indicates the standard oxygen evolution reaction potential.

Based on these dynamics, we posited that an efficient heterojunction system needs to direct charges along process Ⓐ and disfavor off-track routes such as process Ⓑ. Still, solar light includes photons energetic enough to excite WO_3 (~4% of the solar spectrum is at wavelengths below the absorption edge of bulk WO_3). Therefore, a portion of photogenerated charges in $WO_3/BiVO_4$ systems may be wasted through process Ⓑ. On the other hand, $BiVO_4$ efficiently absorbs light beyond the absorption edge of WO_3, up to 520 nm, allowing us to exploit a larger fraction of the solar spectrum. Therefore, in this work we pursue the strategy of using the $BiVO_4$ sensitizer to shield WO_3 from direct photoexcitation.

We assembled a series of heterojunction electrodes with a WO_3 scaffold layer of fixed thickness (ca. 150 nm) coated with $BiVO_4$ overlayers with different thickness (15−160 nm) to tune the amount of light absorbed by $BiVO_4$. First, a systematic PEC study allowed us to probe whether the irradiation mode (through WO_3 or $BiVO_4$, backside or frontside irradiation, respectively, Figure 1B) affects the overall PEC efficiency of the electrodes. Then, transient absorption spectroscopy (TAS) with a pump in the UV region (387 nm) and detection in the visible range was employed to assess the effects of the irradiation mode on the lifetime of photogenerated holes in $BiVO_4$. These tests allowed us to evaluate the extent of charge recombination induced by process Ⓑ and its impact on the PEC performance of the heterojunction photoanodes as a function of the $BiVO_4$ layer thickness.

The $WO_3/BiVO_4$ photoanodes were prepared through spin coating using fluorine-doped tin oxide (FTO) as the conductive glass substrate (see the Supporting Information). The heterojunction electrode with the thickest $BiVO_4$ layer almost entirely absorbs 387 nm photons, the pump wavelength in TAS experiments, Figure 1C. A series of control photoanodes consisting of pure $BiVO_4$ on FTO (without WO_3 layer) with variable $BiVO_4$ thickness was also prepared. The absorption spectra of the two electrode series are shown in Figures S1 and S2; the thickness of the $BiVO_4$ layer was estimated using the absorption coefficient at 420 nm,[19] $\alpha_{40} = 6.7 \times 10^4$ cm^{-1}. XRD analyses confirm the successful synthesis of WO_3 and $BiVO_4$ (Figure S3) and FESEM images

https://doi.org/10.1021/acsaem.2c02597
ACS Appl. Energy Mater. 2022, 5, 13142−13148

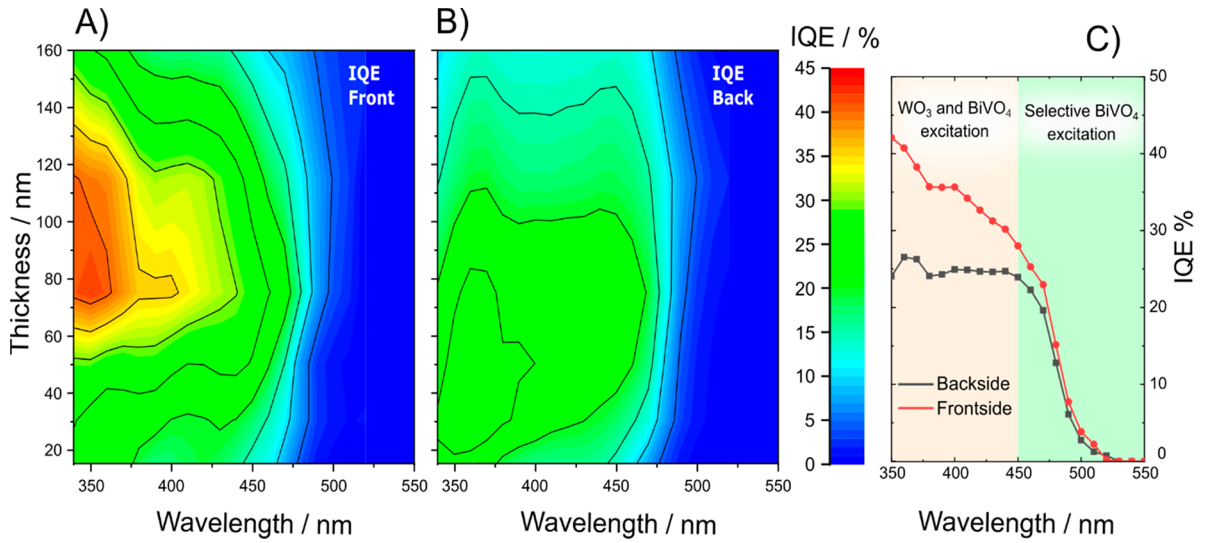

Figure 3. Internal quantum efficiency (IQE) 3D contour plots (color scale) vs the incident wavelength and the $BiVO_4$ film thickness of the WO_3/$BiVO_4$ electrodes, obtained in contact with a 0.5 M Na_2SO_4 aqueous solution at 1.23 V_{SHE} under (A) frontside or (B) backside irradiation; (C) IQE plots under backside and frontside irradiation obtained with the best performing electrode (with a 75 nm thick $BiVO_4$ layer).

demonstrate the uniform coating of the photoanodes (Figure S4).

In order to explore the shielding hypothesis, we carried out PEC experiments on the electrodes. Figure 2A, B shows the photocurrent density generated with the WO_3/$BiVO_4$ electrodes under simulated solar light irradiation in 0.5 M Na_2SO_4 solution under back- and frontside irradiation at different applied potentials. The linear sweep voltammetry plots are reported in Figures S5 and S6. As a general trend, all heterojunction photoanodes outperform control pure $BiVO_4$ electrodes (see Figure S7). Furthermore, the better light exploitation achieved with increasing the $BiVO_4$ layer thickness drives the photocurrent increase under both irradiation conditions up to a 75 nm thick $BiVO_4$ layer.

Under frontside simulated solar light irradiation (Figure 2A), the heterojunction photoanodes generate considerably higher photocurrent than in backside mode (Figure 2B). The best performing electrode with a 75 nm $BiVO_4$ layer thickness (Figure 2C), when irradiated frontside shows a ca. 40% increase in the current density, from 1.0 to 1.38 mA cm^{-2}, with respect to backside irradiation, at the formal H_2O/O_2 redox potential of 1.23 V vs the standard hydrogen electrode (V_{SHE}).

We used single-wavelength efficiency measurements to gather further information on this PEC performance increase. Specifically, internal quantum efficiency (IQE, Figure 3 and Figures S8 and S9), measuring the efficiency of absorbed photons, was calculated from the incident photon to current efficiency (IPCE, see Figures S10 and S11) recorded with the WO_3/$BiVO_4$ electrodes in contact with a 0.5 M Na_2SO_4 solution at 1.23 V_{SHE}. Figure 3A, B shows the IQE vs $BiVO_4$ thickness contour plots measured under frontside and backside irradiation.

Under frontside irradiation, the IQE reaches the highest values for 70−130 nm thick $BiVO_4$ layers in the WO_3/$BiVO_4$ heterojunction, as evidenced by the red/yellow island appearing in Figure 3A as opposed to the green plot obtained under backside irradiation, which leads to lower IQE values (Figure 3B). Notably, the largest IQE enhancement under frontside irradiation occurs below 450 nm, where WO_3 absorbs light, and for $BiVO_4$ layers thicker than 50 nm, which absorb a substantial fraction of incident light. The IQE in this irradiation mode maintains above 30% up to 450 nm for the best-performing electrodes, while it is seldom above 25% under backside irradiation, see for example the IQE traces for the WO_3/$BiVO_4$ electrode with 75 nm thick $BiVO_4$ in Figure 3C.

At the same time, the IQE curves are similar under the two irradiation modes in the 450−520 nm range because only $BiVO_4$ absorbs light at these wavelengths and process Ⓐ (Figure 1A) is predominantly active. Thus, these wavelength-dependent PEC analyses indicate that the performance of the WO_3/$BiVO_4$ photoanodes benefits from avoiding WO_3 excitation. This condition occurs by selectively exciting $BiVO_4$ under frontside irradiation, i.e., by shielding WO_3 with $BiVO_4$, and in both irradiation modes under excitation at wavelengths above the WO_3 absorption onset (Figure 3C).

We then investigated the effect of WO_3 shielding on the lifetime of photogenerated holes in the $BiVO_4$ layer of the WO_3/$BiVO_4$ system. Previous work ascribed the transient absorption ΔA signal at 470 nm to trapped holes in $BiVO_4$, based on experiments in the presence of hole scavengers.[18,21,31] TAS proved an essential tool for studying charge carrier dynamics and diffusion in photocatalysis and photovoltaics.[32−35] Therefore, TAS with detection at 470 nm was here employed to investigate the dynamics of photogenerated holes in both pure $BiVO_4$ and WO_3/$BiVO_4$ electrode series upon backside and frontside excitation at 387 nm.

The ΔA signals recorded with pure $BiVO_4$ electrodes were analyzed first. For this system, similar transient dynamics were obtained in the two irradiation modes. Figure S12 reports representative transient absorption spectra, while Figure S13 shows the transient decay ΔA profiles at 470 nm, which were fitted according to a biexponential decay model (eq 1).

$$\Delta A = A_1 e^{-t/\tau_1} + A_2 e^{-t/\tau_2} + \Delta A_0 \quad (1)$$

In this equation, τ_1 and τ_2 are the lifetimes of the faster and slower decay processes typical of $BiVO_4$, respectively, A_1 and A_2 are the weighted coefficients that represent the contribution of each of the two processes to the overall decay and ΔA_0 is the offset (set at zero in the fitting).[21] The fitting parameters for the $BiVO_4$ electrodes (Table S1) are in line with literature

https://doi.org/10.1021/acsaem.2c02597
ACS Appl. Energy Mater. 2022, 5, 13142−13148

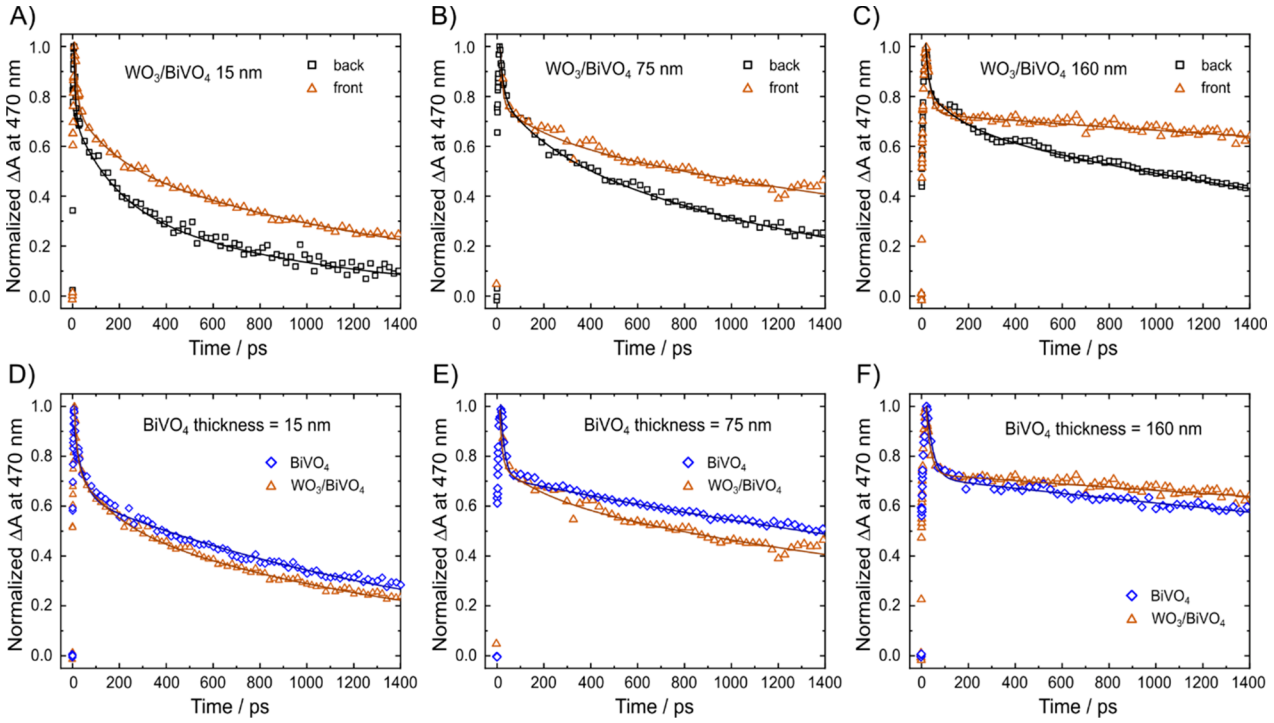

Figure 4. Comparison between the normalized TAS decay signals in (A–C) $WO_3/BiVO_4$ electrodes with different $BiVO_4$ thicknesses recorded under backside (through WO_3, black squares) or frontside (through $BiVO_4$, red triangles) irradiation and in (D–F) $WO_3/BiVO_4$ (red triangles) and pure $BiVO_4$ films (blue diamonds) with the same $BiVO_4$ thickness recorded under frontside irradiation. The solid lines are the fitting curves according to eq 1 ($BiVO_4$ films) or eq 2 ($WO_3/BiVO_4$ films). Excitation pump at 387 nm, TAS signal monitored at 470 nm.

Table 1. Fitting Parameters of the TAS Dataset Collected with the $WO_3/BiVO_4$ Electrodes under Backside Excitation at 387 nm[a]

$BiVO_4$ thickness (nm)	A_1 (%)	τ_1 (ps)	A_r (%)	τ_r (ps)	A_2 (%)	τ_2 (ns)
15	30 ± 1	7.4 ± 0.8	32 ± 3	170 ± 22	38 ± 3	0.98 ± 0.07
30	26 ± 2	6.2 ± 1.1	34 ± 3	189 ± 27	40 ± 3	1.9 ± 0.2
50	24 ± 2	7.8 ± 1.2	19 ± 2	156 ± 30	57 ± 2	1.99 ± 0.11
75	22 ± 1	15.8 ± 1.8	17 ± 2	215 ± 48	61 ± 3	1.44 ± 0.07
115	23 ± 2	22 ± 3	19 ± 2	210 ± 25	58.0 ± 0.3	3.57 ± 0.11
160	18 ± 1	13.1 ± 1.7	15 ± 1	159 ± 26	67.4 ± 0.9	3.05 ± 0.11

[a]Data fitted according to eq 2.

reports on pure $BiVO_4$. Regardless of the $BiVO_4$ thickness , A_1 and A_2 account of ~30 and 70% of the hole decay, respectively. The fast decay lifetime, which is associated with the recombination of trapped holes in $BiVO_4$ with photopromoted free electrons, is independent of the $BiVO_4$ layer thickness (τ_1, ~20 ps), because all electrodes are excited at the same pump wavelength (i.e., with the same energy excess with respect to the $BiVO_4$ CB).[21,29] On the other hand, τ_2, which is ascribed to the recombination of trapped holes with trapped electrons, increases from ~1 to 6.5 ns with increasing $BiVO_4$ layer thickness as more holes get trapped in bulk sites.[28,36,37]

The decay signal of photoproduced holes in the $BiVO_4$ layer of the $WO_3/BiVO_4$ electrodes series recorded at 470 nm under backside and frontside irradiation are reported in Figure 4 and Figures S14 and S15. Under frontside excitation, the ΔA signals decay slower than under backside excitation (Figure 4A–C). Indeed, under backside irradiation mode a significant fraction of 387 nm photons is absorbed by WO_3, leading to photoexcitation of electrons into its CB (the individual WO_3 layer absorbs ca. 16% of 387 photons, Figure 1C). Therefore, many photoproduced charge carriers recombine through process Ⓑ (Figure 1A). This additional recombination channel leads to the abrupt ΔA drop observed during the first 400 ps following backside photoexcitation (Figure 4A). Furthermore, under frontside irradiation the ΔA signal recorded with the $WO_3/BiVO_4$ heterojunctions becomes progressively slower and comparable with those recorded with pure $BiVO_4$ (Figure 4D–F and Figure S13).

In previous studies on the $WO_3/BiVO_4$ heterojunction, we evaluated the contribution of process Ⓑ to the overall ΔA decay signal by fitting the ΔA decay traces including an additional decay component in eq 1, to take into account also process Ⓑ.[26] Here, we used the same approach to assess its contribution to the charge carrier dynamics in the two irradiation modes and fitted the ΔA decay with eq 2.

$$\Delta A = A_1 e^{-t/\tau_1} + A_2 e^{-t/\tau_2} + A_r e^{-t/\tau_r} + \Delta A_0 \quad (2)$$

where τ_r accounts for the additional recombination process and A_r is its weighted contribution.

We first fitted the dynamics recorded in the $WO_3/BiVO_4$ electrodes under backside excitation. The fitting parameters are reported in Table 1. In this configuration, the WO_3 layer is

https://doi.org/10.1021/acsaem.2c02597
ACS Appl. Energy Mater. 2022, 5, 13142–13148

Table 2. Fitting Parameters of the TAS Dataset Collected with the $WO_3/BiVO_4$ Electrodes under Frontside Excitation at 387 nm[a]

$BiVO_4$ thickness (nm)	A_1 (%)	τ_1 (ps)	A_r (%)	τ_r (ps)	A_2 (%)	τ_2 (ns)
15	25 ± 1	13 ± 1	20 ± 1	170	55 ± 1	1.55 ± 0.03
30	23 ± 3	15 ± 2	27 ± 3	189	50 ± 3	2.8 ± 0.4
50	21 ± 3	19 ± 7	13 ± 5	156	66 ± 2	3.0 ± 0.3
75	23 ± 3	10 ± 3	12 ± 4	215	65 ± 2	3.1 ± 0.4
115	20 ± 1	24 ± 4	4 ± 2	210	76.3 ± 0.8	5.4 ± 0.3
160	27 ± 1	21 ± 2	-	-	73.1 ± 0.3	10.6 ± 1.2

[a]Data fitted according to eq 2 using the τ_r values reported in Table 1.

irradiated directly and absorbs the same amount of light in all electrodes. Therefore, we expect that process Ⓑ has a comparable effect on the charge carrier dynamics at each $BiVO_4$ layer thickness. Indeed, this process accounts for ca. 23 ± 8% of the holes decay, with a time constant τ_r of ∼200 ps (Table 1).

Under frontside irradiation, the $BiVO_4$ layer in the heterojunction electrodes shields WO_3 from light absorption as the $BiVO_4$ layer thickness increases. Indeed, the percent amount of incident 387 nm photons absorbed by the WO_3 underlayer in the coupled system progressively decreases (Figure 1C). Therefore, we sought to quantify the shielding effect of the $BiVO_4$ layer in decreasing the extent of process Ⓑ in the $WO_3/BiVO_4$ electrodes. By assuming that process Ⓑ operates with its intrinsic time constant τ_r regardless of the excitation mode, we fitted the decay dynamics recorded under frontside irradiation by employing the τ_r previously extracted from the TAS signals recorded upon excitation in backside mode (Table 1). Because of the reduced amount of charge carriers generated in WO_3, the weight of process Ⓑ in terms of the A_r parameter (Table 2) decreases with increasing the $BiVO_4$ layer thickness. Additionally, as fewer charge carriers undergo process Ⓑ, A_2 increases, suggesting that a larger number of photogenerated charge carriers recombines through the slower process. A 160 nm thick $BiVO_4$ layer almost entirely absorbs the pump (Figure 1C), preventing WO_3 excitation. Due to the lack of photoexcited electrons in the CB of WO_3, the electrons photopromoted in the $BiVO_4$ CB can only recombine with trapped holes in $BiVO_4$, or flow into WO_3 CB via process Ⓐ, resulting in better charge carrier separation. Consequently, the holes photogenerated in the $BiVO_4$ layer of the $WO_3/BiVO_4$ heterojunction live longer than those in the individual 160 nm thick $BiVO_4$ electrode (Figure 4F). This condition is akin to selective $BiVO_4$ excitation in $WO_3/BiVO_4$ at wavelengths beyond WO_3 absorption edge, which we previously observed extending the hole lifetimes compared to individual $BiVO_4$.[26,29]

Thus, TAS and PEC experiments suggest that light absorption by the $BiVO_4$ layer in $WO_3/BiVO_4$ electrodes selectively suppresses process Ⓑ and promotes process Ⓐ, which leads to an increase of trapped hole lifetime in $BiVO_4$. However, despite the promise of long-living holes in the heterojunction electrode with a 160 nm thick $BiVO_4$ layer, it performs poorly compared to the most active heterojunction with the 75 nm thick $BiVO_4$ layer. This latter electrode possesses an optimal matching between (i) WO_3 sensitization to the visible light, (ii) photogenerated charge separation at the heterojunction, and (iii) efficient charge extraction toward the external circuit and the electrolyte. Indeed, thinner $BiVO_4$ layers limit the electrode performance due to the low visible light absorption, while thicker films may suffer from a greater charge recombination owing to hole accumulation in the $BiVO_4$ bulk under *operando* conditions.

In conclusion, we identified a shielding strategy to suppress the internal charge recombination occurring in the $WO_3/BiVO_4$ heterojunction due to WO_3 excitation. Optimized light absorption in $BiVO_4$ layers considerably suppresses this recombination channel. The best performing electrode tested in this work shows a 40% increase in the PEC performance under frontside irradiation compared to backside irradiation. Furthermore, these findings suggest that methods to suppress undesired wavelength-dependent recombination processes and optimize charge transport and surface catalysis are required to design efficient photoelectrodes based on type-II heterojunctions.

■ ASSOCIATED CONTENT

Supporting Information

The Supporting Information is available free of charge at https://pubs.acs.org/doi/10.1021/acsaem.2c02597.

Experimental details, absorption spectra, XRD and FESEM analyses, linear sweep voltammetry tests, IQE and IPCE plots, TAS decay profiles, and fitting parameters (PDF)

■ AUTHOR INFORMATION

Corresponding Authors

Ivan Grigioni − *Dipartimento di Chimica, Università degli Studi di Milano, Milano 20133, Italy;* orcid.org/0000-0002-9469-4570; Email: ivan.grigioni@unimi.it

Elena Selli − *Dipartimento di Chimica, Università degli Studi di Milano, Milano 20133, Italy;* orcid.org/0000-0001-8391-7639; Email: elena.selli@unimi.it

Authors

Annalisa Polo − *Dipartimento di Chimica, Università degli Studi di Milano, Milano 20133, Italy;* orcid.org/0000-0001-5724-2607

Maria Vittoria Dozzi − *Dipartimento di Chimica, Università degli Studi di Milano, Milano 20133, Italy;* orcid.org/0000-0002-6390-9348

Kevin G. Stamplecoskie − *Department of Chemistry, Queen's University, Kingston, Ontario K7L 3N6, Canada;* orcid.org/0000-0002-0232-9956

Danilo H. Jara − *Facultad de Ingeniería y Ciencias, Universidad Adolfo Ibáñez, Viña del Mar 7941169, Chile;* orcid.org/0000-0001-9752-4465

Prashant V. Kamat − *Radiation Laboratory, University of Notre Dame, Notre Dame, Indiana 46556, United States;* orcid.org/0000-0002-2465-6819

Complete contact information is available at:

https://doi.org/10.1021/acsaem.2c02597
ACS Appl. Energy Mater. 2022, 5, 13142−13148

https://pubs.acs.org/10.1021/acsaem.2c02597

Notes

The authors declare no competing financial interest.

■ ACKNOWLEDGMENTS

I.G. acknowledges the European Union's Horizon 2020 research and innovation programme under the Marie Sklodowska-Curie Grant Agreement 846107. This work received financial support from the MIUR PRIN 20173397R7MULTI-e project. The use of instrumentation purchased through the Regione Lombardia-Fondazione Cariplo joint SmartMatLab project (Fondazione Cariplo grant 2013-1766) is gratefully acknowledged. P.V.K. acknowledges the support of the Division of Chemical Sciences, Geosciences, and Biosciences, Office of Basic Energy Sciences of the U.S. Department of Energy, through award DE-FC02-04ER15533. This is contribution number NDRL 5380 from the Notre Dame Radiation Laboratory.

■ REFERENCES

(1) Park, Y.; Mc Donald, K. J.; Choi, K. S. Progress in Bismuth Vanadate Photoanodes for Use in Solar Water Oxidation. *Chem. Soc. Rev.* **2013**, *42*, 2321−2337.

(2) Sivula, K.; Van De Krol, R. Semiconducting Materials for Photoelectrochemical Energy Conversion. *Nat. Rev. Mater.* **2016**, *1*, 15010.

(3) Lee, D. K.; Choi, K. S. Enhancing Long-Term Photostability of $BiVO_4$ Photoanodes for Solar Water Splitting by Tuning Electrolyte Composition. *Nat. Energy* **2018**, *3*, 53−60.

(4) Kuang, Y.; Jia, Q.; Ma, G.; Hisatomi, T.; Minegishi, T.; Nishiyama, H.; Nakabayashi, M.; Shibata, N.; Yamada, T.; Kudo, A.; Domen, K. Ultrastable Low-Bias Water Splitting Photoanodes via Photocorrosion Inhibition and in Situ Catalyst Regeneration. *Nat. Energy* **2017**, *2*, 16191.

(5) Kudo, A.; Ueda, K.; Kato, H.; Mikami, I. Photocatalytic O_2 Evolution under Visible Light Irradiation on $BiVO_4$ in Aqueous $AgNO_3$ Solution. *Catal. Lett.* **1998**, *53*, 229−230.

(6) Abdi, F. F.; Han, L.; Smets, A. H. M.; Zeman, M.; Dam, B.; Van De Krol, R. Efficient Solar Water Splitting by Enhanced Charge Separation in a Bismuth Vanadate-Silicon Tandem Photoelectrode. *Nat. Commun.* **2013**, *4*, 2195.

(7) Liu, H.; Nakamura, R.; Nakato, Y. Promoted Photo-Oxidation Reactivity of Particulate $BiVO_4$ Photocatalyst Prepared by a Photoassisted Sol-Gel Method. *J. Electrochem. Soc.* **2005**, *152*, G856.

(8) Gao, R. T.; Wang, L. Stable Cocatalyst-Free $BiVO_4$ Photoanodes with Passivated Surface States for Photocorrosion Inhibition. *Angew. Chemie - Int. Ed.* **2020**, *59*, 23094−23099.

(9) Kim, T. W.; Choi, K.-S. Nanoporous $BiVO_4$ Photoanodes with Dual-Layer Oxygen Evolution Catalysts for Solar Water Splitting. *Science.* **2014**, *343*, 990−994.

(10) Zhang, X.; Zhai, P.; Zhang, Y.; Wu, Y.; Wang, C.; Ran, L.; Gao, J.; Li, Z.; Zhang, B.; Fan, Z.; Sun, L.; Hou, J. Engineering Single-Atomic Ni-N_4-O Sites on Semiconductor Photoanodes for High-Performance Photoelectrochemical Water Splitting. *J. Am. Chem. Soc.* **2021**, *143*, 20657−20669.

(11) Seabold, J. A.; Choi, K. S. Efficient and Stable Photo-Oxidation of Water by a Bismuth Vanadate Photoanode Coupled with an Iron Oxyhydroxide Oxygen Evolution Catalyst. *J. Am. Chem. Soc.* **2012**, *134*, 2186−2192.

(12) Gao, Y.; Tian, Z.; Zhu, H.; Xue, H.; Ma, L.; Dai, Y.; Zhao, W.; Li, X.; Li, N.; Ge, L. In Situ Activation of Amorphous NiFeMo Oxide Cocatalyst to Improve the Photoelectrochemical Water Splitting Performance of $BiVO_4$. *ACS Appl. Energy Mater.* **2021**, *4*, 14649−14661.

(13) Fang, W.; Fu, L.; Qin, A.; Lin, Y.; Xv, R. Highly Active and Self-Healing Co-Doped $BiVO_4$ Photoanode in Borate Buffer to Enhance Charge Separation and Water Oxidation Kinetics during Photoelectrochemical Water Splitting. *ACS Appl. Energy Mater.* **2022**, *5*, 6313−6323.

(14) Abdi, F. F.; Savenije, T. J.; May, M. M.; Dam, B.; Van De Krol, R. The Origin of Slow Carrier Transport in $BiVO_4$ Thin Film Photoanodes: A Time-Resolved Microwave Conductivity Study. *J. Phys. Chem. Lett.* **2013**, *4*, 2752−2757.

(15) Hong, S. J.; Lee, S.; Jang, J. S.; Lee, J. S. Heterojunction $BiVO_4$/WO_3 Electrodes for Enhanced Photoactivity of Water Oxidation. *Energy Environ. Sci.* **2011**, *4*, 1781−1787.

(16) Shi, X.; Jeong, H.; Oh, S. J.; Ma, M.; Zhang, K.; Kwon, J.; Choi, I. T.; Choi, I. Y.; Kim, H. K.; Kim, J. K.; Park, J. H. Unassisted Photoelectrochemical Water Splitting Exceeding 7% Solar-to-Hydrogen Conversion Efficiency Using Photon Recycling. *Nat. Commun.* **2016**, *7*, 11943.

(17) Pihosh, Y.; Turkevych, I.; Mawatari, K.; Uemura, J.; Kazoe, Y.; Kosar, S.; Makita, K.; Sugaya, T.; Matsui, T.; Fujita, D.; et al. Photocatalytic Generation of Hydrogen by Core-Shell WO_3/$BiVO_4$ Nanorods with Ultimate Water Splitting Efficiency. *Sci. Rep.* **2015**, *5*, 11141.

(18) Grigioni, I.; Stamplecoskie, K. G.; Selli, E.; Kamat, P. V. Dynamics of Photogenerated Charge Carriers in WO_3/$BiVO_4$ Heterojunction Photoanodes. *J. Phys. Chem. C* **2015**, *119*, 20792−20800.

(19) Grigioni, I.; Di Liberto, G.; Dozzi, M. V.; Tosoni, S.; Pacchioni, G.; Selli, E. WO_3/$BiVO_4$ Photoanodes: Facets Matching at the Heterojunction and $BiVO_4$ Layer Thickness Effects. *ACS Appl. Energy Mater.* **2021**, *4*, 8421−8431.

(20) Liu, Y.; Wygant, B. R.; Kawashima, K.; Mabayoje, O.; Hong, T. E.; Lee, S. G.; Lin, J.; Kim, J. H.; Yubuta, K.; Li, W.; Li, J.; Mullins, C. B. Facet Effect on the Photoelectrochemical Performance of a WO_3/$BiVO_4$ Heterojunction Photoanode. *Appl. Catal. B Environ.* **2019**, *245*, 227−239.

(21) Ravensbergen, J.; Abdi, F. F.; Van Santen, J. H.; Frese, R. N.; Dam, B.; Van De Krol, R.; Kennis, J. T. M. Unraveling the Carrier Dynamics of $BiVO_4$: A Femtosecond to Microsecond Transient Absorption Study. *J. Phys. Chem. C* **2014**, *118*, 27793−27800.

(22) Ma, Y.; Pendlebury, S. R.; Reynal, A.; Le Formal, F.; Durrant, J. R. Dynamics of Photogenerated Holes in Undoped $BiVO_4$ Photoanodes for Solar Water Oxidation. *Chem. Sci.* **2014**, *5*, 2964−2973.

(23) Selim, S.; Francàs, L.; García-Tecedor, M.; Corby, S.; Blackman, C.; Gimenez, S.; Durrant, J. R.; Kafizas, A. WO_3/$BiVO_4$: Impact of Charge Separation at the Timescale of Water Oxidation. *Chem. Sci.* **2019**, *10*, 2643−2652.

(24) Ma, Y.; Mesa, C. A.; Pastor, E.; Kafizas, A.; Francàs, L.; Le Formal, F.; Pendlebury, S. R.; Durrant, J. R. Rate Law Analysis of Water Oxidation and Hole Scavenging on a $BiVO_4$ Photoanode. *ACS Energy Lett.* **2016**, *1*, 618−623.

(25) Venugopal, A.; Kas, R.; Hau, K.; Smith, W. A. Operando Infrared Spectroscopy Reveals the Dynamic Nature of Semiconductor-Electrolyte Interface in Multinary Metal Oxide Photoelectrodes. *J. Am. Chem. Soc.* **2021**, *143*, 18581−18591.

(26) Grigioni, I.; Stamplecoskie, K. G.; Jara, D. H.; Dozzi, M. V.; Oriana, A.; Cerullo, G.; Kamat, P. V.; Selli, E. Wavelength-Dependent Ultrafast Charge Carrier Separation in the WO_3/$BiVO_4$ Coupled System. *ACS Energy Lett.* **2017**, *2*, 1362−1367.

(27) Grigioni, I.; Ganzer, L.; Camargo, F. V. A.; Bozzini, B.; Cerullo, G.; Selli, E. In Operando Photoelectrochemical Femtosecond Transient Absorption Spectroscopy of WO_3/$BiVO_4$ Heterojunctions. *ACS Energy Lett.* **2019**, *4*, 2213−2219.

(28) Polo, A.; Dozzi, M. V.; Grigioni, I.; Lhermitte, C.; Plainpan, N.; Moretti, L.; Cerullo, G.; Sivula, K.; Selli, E. Multiple Effects Induced by Mo^{6+} Doping in $BiVO_4$ Photoanodes. *Sol. RRL* **2022**, *6*, 2200349.

(29) Grigioni, I.; Abdellah, M.; Corti, A.; Dozzi, M. V.; Hammarström, L.; Selli, E. Photoinduced Charge-Transfer Dynamics in WO_3/$BiVO_4$ Photoanodes Probed through Midinfrared Transient Absorption Spectroscopy. *J. Am. Chem. Soc.* **2018**, *140*, 14042−14045.

(30) Grigioni, I.; Dozzi, M. V.; Selli, E. Photoinduced Electron Transfer in WO_3/$BiVO_4$ Heterojunction Photoanodes: Effects of the WO_3 Layer Thickness. *J. Phys.: Condens. Matter* **2020**, *32*, 014001.
(31) Suzuki, Y.; Murthy, D. H. K.; Matsuzaki, H.; Furube, A.; Wang, Q.; Hisatomi, T.; Domen, K.; Seki, K. Rational Interpretation of Correlated Kinetics of Mobile and Trapped Charge Carriers: Analysis of Ultrafast Carrier Dynamics in $BiVO_4$. *J. Phys. Chem. C* **2017**, *121*, 19044−19052.
(32) Christians, J. A.; Leighton, D. T.; Kamat, P. V. Rate Limiting Interfacial Hole Transfer in Sb_2S_3 Solid-State Solar Cells. *Energy Environ. Sci.* **2014**, *7*, 1148−1158.
(33) Christians, J. A.; Kamat, P. V. Trap and Transfer. Two-Step Hole Injection across the Sb_2S_3/CuSCN Interface in Solid-State Solar Cells. *ACS Nano* **2013**, *7*, 7967−7974.
(34) Stranks, S. D.; Eperon, G. E.; Grancini, G.; Menelaou, C.; Alcocer, M. J. P.; Leijtens, T.; Herz, L. M.; Petrozza, A.; Snaith, H. J. Electron-Hole Diffusion Lengths Exceeding Trihalide Perovskite Absorber. *Science* **2013**, *342*, 341−344.
(35) Cowan, A. J.; Durrant, J. R. Long-Lived Charge Separated States in Nanostructured Semiconductor Photoelectrodes for the Production of Solar Fuels. *Chem. Soc. Rev.* **2013**, *42*, 2281−2293.
(36) Pattengale, B.; Huang, J. Implicating the Contributions of Surface and Bulk States on Carrier Trapping and Photocurrent Performance of $BiVO_4$ Photoanodes. *Phys. Chem. Chem. Phys.* **2017**, *19*, 6831−6837.
(37) Polo, A.; Grigioni, I.; Magni, M.; Facibeni, A.; Dozzi, M. V.; Selli, E. Unravelling the Bulk and Interfacial Charge Transfer Effects of Molybdenum Doping in $BiVO_4$ Photoanodes. *Appl. Surf. Sci.* **2021**, *556*, 149759.

https://doi.org/10.1021/acsaem.2c02597
ACS Appl. Energy Mater. 2022, 5, 13142−13148